New Torque and Flux Controllers for Direct Torque Control of Induction Machines

C. L. Toh, N. R. N Idris, A. H. M Yatim
Department of Energy Conversion, University Teknologi Malaysia, Malaysia

Abstract—**The new torque and flux controllers with constant switching frequency and low torque and flux ripples for direct torque control induction machine drives are presented. The core of these proposed controllers is based on the comparison between the compensated error signals with high frequency triangular waveforms, thus does not require complex calculation to generate the inverter switching signals. The controllers are therefore can be implemented using analog and/or digital circuits. Modeling and simulation of the new controllers are presented and the results show that the torque and flux ripples are reduced significantly.**

Keywords—**DTC, motor drives, torque ripple**

I. Introduction

The applications of Direct Torque Control (DTC) induction motor drives are gradually increasing. In some applications, they are replacing the vector control drives normally found in industry applications [1]. The core of this control method is to minimize the torque and flux errors to zero by using a pair of hysteresis comparators.

The hysteresis comparators lie at the heart of DTC scheme not only to determine the appropriate voltage vector selection but also the period of the voltage vector remains selected. In order to maintain the flux and torque errors within the fix hysteresis bands, the switching frequency becomes variable and unpredictable. The switching frequency varies with the operating speed, load condition and parameters of the induction machine [4,5]. Hence to ensure the switching frequency does not exceed the limit we have to calculate the extreme cases corresponding to the maximum switching frequency. Nevertheless the drive does not operate in these extreme cases in most of the time therefore the switching capability is not fully utilized. To overcome this problem, a number of literature papers had been proposed. Basically they can be divided into hysteresis based and non-hysteresis based solutions. In [6] variable hysteresis band comparators had been designed where the band can be adjusted to fix the switching frequency. For non-hysteresis based, the main idea is to predict the duty cycle of the switching device based on the torque and flux errors, the transient reactance of the machine and an estimated value of the voltage behind the transient reactance [7]. The torque controller will switch at regular intervals thus ensuring constant switching frequency of the inverter. A few techniques have been proposed, including the use of space vector modulation, predictive control schemes and intelligent control techniques, which had been published in [7–12]. All in all, the above solutions involved complex calculation and this will increase the complexity of the DTC drive.

Another problem that is normally associated with DTC drive is the high torque ripple. Ideally, small torque hysteresis band will produce small torque ripple. However, for microprocessor-based implementation, if the hysteresis band is set too small, the torque may overshoot and touch the upper band. Once it touches the upper band the hysteresis comparator will produce a signal that will select a reverse voltage vector instead of zero voltage vector to reduce the torque [3,5]. Due to this incorrect voltage vector selection, the undershoot may occur and as a result, the torque ripple is increased drastically. In [13], it is shown that for microprocessor-based implementation, the torque ripple can be reduced significantly by reducing the sampling period. In other words, the undesired overshoot or undershoot in torque can be minimized by employing a faster sampling period. The non-hysteresis based control technique had increased the burden of the processor to calculate the appropriate duty cycles or voltage vector with the aim to reduce the sampling time. In [14], it is highlighted that the delay in estimating the flux and torque become the root cause where the switching frequency cannot be raised. In order to overcome this problem a dithering technique has been proposed by superposing triangular wave with high frequency and minute amplitude on the flux and torque errors. This technique had increased the switching frequency effectively and minimized the torque and flux ripples significantly.

Recently, a new torque controller, which produces constant torque switching frequency with low ripple, has been presented in [15]. It replaces the convention hysteresis comparator with a fixed switching frequency controller. A fixed switching frequency is obtained by comparing the triangular waveforms with the compensated error signals. However, there are two major limitations associated with this method. Firstly, the switching frequency is limited by the sampling period of the processor. Secondly, the switching frequency still vary due to the flux hysteresis comparator. In this paper, a new torque and flux controllers are presented to overcome these limitations. The operations of the new torque and flux controllers are similar to the torque controller proposed in [15] but, with a much higher triangular waveforms frequencies. The maximum switching capability of the devices can be fully utilized since the switching frequency is independent from the operating conditions and equals the triangular waveform frequency. These controllers are easy to implement by utilizing digital circuit since it just involves comparison of

waveform rather than complicated calculation of duty cycles or voltage vector. The rest of the paper is organized as follows. Section II gives the torque and flux equations. Section III represents the proposed controllers and the controllers' design is shown in section IV. Section V outlines the parameters of the controller and shows the simulation result. Finally, section VI draws the conclusions.

II. Torque And Flux Equations

The dynamic behavior of an induction machine is described by the following equations written in terms of space vectors in stationary stator reference frame

$$\bar{v}_s = R_s \bar{i}_s + \frac{d\bar{\psi}_s}{dt} \tag{1}$$

$$0 = R_r \bar{i}_r + \frac{d\bar{\psi}_r}{dt} - j\omega_m \bar{\psi}_r \tag{2}$$

$$\bar{\psi}_s = L_s \bar{i}_s + L_m \bar{i}_r \tag{3}$$

$$\bar{\psi}_r = L_r \bar{i}_r + L_m \bar{i}_s \tag{4}$$

where $\bar{v}_s$ stator voltage
$\bar{i}_s, \bar{i}_r$ stator and rotor current
R_s, R_r stator and rotor resistance
L_s, L_r stator and rotor self inductance
L_m mutual inductance
$\bar{\psi}_s, \bar{\psi}_r$ stator and rotor flux
ω_m motor angular velocity

The torque, T_e and mechanical dynamics of the machine are modeled as followed:

$$T_e = \frac{3}{2}\frac{p}{2}\bar{\psi}_s \times \bar{i}_s \tag{5}$$

$$J\frac{d\omega_m}{dt} = J\frac{2}{p}\frac{d\omega_r}{dt} = T_e - T_{load} \tag{6}$$

In [16], it is highlighted that the torque slope is a function of motor speed, stator and rotor fluxes, and stator voltage. As derived in [16], the equations of the positive and negative slope are presented in (7) and (8) respectively.

$$\frac{dT_e^+}{dt} = -\frac{T_e}{\sigma\tau_{sr}} + \frac{3}{4}\frac{p}{\sigma L_s L_r}\left(\bar{v}_s - j\omega_r\bar{\psi}_s\right)\cdot j\bar{\psi}_r \tag{7}$$

$$\frac{dT_e^-}{dt} = -\frac{T_e}{\sigma\tau_{sr}} - \frac{3}{4}\frac{p}{\sigma L_s L_r} j\omega_r\bar{\psi}_s \cdot j\bar{\psi}_r \tag{8}$$

where σ is the leakage coefficient, $\sigma = 1 - \frac{L_m^2}{L_s L_r}$

By rearranging (1), the slope of flux in stator reference frame can be written as:

$$\frac{d\bar{\psi}_s}{dt} = \bar{v}_s - i_s R_s \tag{9}$$

Analysis is simplified if the stator resistance voltage drop is neglected; hence the flux variation direction is fixed along the selected voltage vector. If the stator flux lies in sector k as shown in Fig. 1, then the voltage vector $v_{s,k+1}$ or v_{sk+2} will be selected to increase or decrease the stator flux. The positive and negative slopes are given by [16]:

$$\frac{d\bar{\psi}_s^+}{dt} = \frac{2}{3}V_{dc}\sin\theta, \left(0 \le \theta \le \frac{\pi}{3}\right) \tag{10}$$

$$\frac{d\bar{\psi}_s^-}{dt} = -\frac{2}{3}V_{dc}\sin\left(\theta + \frac{2\pi}{3}\right), \left(0 \le \theta \le \frac{\pi}{3}\right) \tag{11}$$

where θ is and angle between the stator flux locus and the selected voltage vector. Equation (10) and (11) show that the increase and decrease of the stator flux magnitude is highly nonlinear because of the sinusoidal functions with respect to stator flux angle θ.

III. Proposed Controllers

The idea of fixed switching frequency originated from the fixed frequency current regulator that compares the fixed frequency triangular waveform with the error signal. By replacing the hysteresis controllers with the proposed controllers will result in a high and constant switching frequency. It is believed that the switching frequency can be set above the audible range, i.e. greater than 20 kHz. With the high switching frequency, the torque and flux ripples are further minimized.

A. Torque Controller

The controller consists of two triangular waveform generators, two comparators and a PI controller as shown in Fig.2. The two triangular waveforms (C_{upper} and C_{lower}) are 180° out of phase with each other. The absolute values of the DC offsets for the triangular waveforms are set to half of their peak-peak values. The instantaneous output of the proposed torque controller, $q_t(t)$ is same as the three level hysteresis comparator [2], that can be one of the three states: –1, 0 or 1 with the following conditions.

$$q_t(t) = \begin{cases} 1 & \text{for } T_c > C_{upper} \\ 0 & \text{for } C_{lower} < T_c < C_{upper} \\ -1 & \text{for } T_c > C_{lower} \end{cases} \tag{12}$$

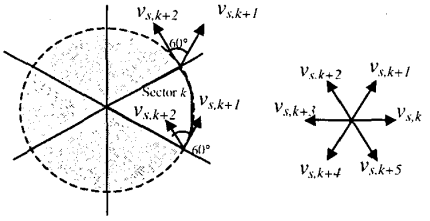

Fig. 1. Selection of voltage vectors in sector k

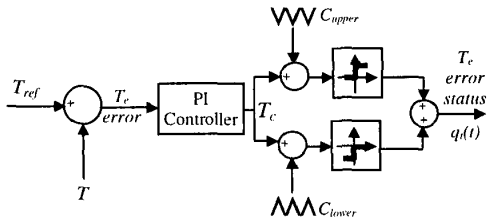

Fig. 2. Proposed torque controller

The average torque error status is defined as continuous duty ratio and is denoted by $d(t)$. The average is taken over an interval T_{tri}, which is the period of the triangular carrier waveform.

$$d_f(t) = \frac{1}{T_{tri}} \int_{t}^{t+T_{tri}} q(t)\, dt \tag{13}$$

B. Flux Controller

Fig. 3 outlines the propose flux controller which in principle works similar to the torque controller. Since the instantaneous output of flux controller is either 1 or 0, only one triangular waveform is required. Equation (14) and (15) are the flux error status and its average value, respectively

$$q_f(t) = \begin{cases} 1 & for\ F_c \geq C_{upper} \\ 0 & for\ F_c < C_{lower} \end{cases} \tag{14}$$

$$d_f(t) = \frac{1}{T_{tri}} \int_{t}^{t+T_{tri}} q(t)\, dt \tag{15}$$

IV Controllers Design

The proposed controllers are designed step-by-step, starting from modeling, averaging and linearizing the respective loop. Linear control system theory is the fundamental of the design.

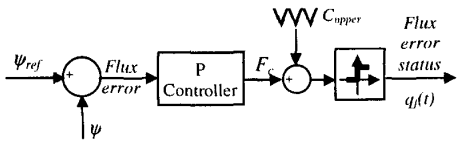

Fig. 3. Proposed flux controller

A. Torque Controller

The relation between $d(t)$ and T_c is just simply a pure gain with a value equals the reciprocal of the peak-peak value of the triangular carrier [15].

In order to simplify the averaging and linearization of the torque equations in (7) and (8), they are defined in the stator flux reference. Two assumptions are made as follows [15]. It is assumed that the applied voltage vector is tangential to the circular locus of the stator flux. Further, it is also assumed that the magnitude of the d component of the rotor flux equals the modulus of the rotor flux. Thus (7) and (8) become:

$$\frac{dT_e^+}{dt} = -\frac{T_e}{\sigma\tau_{sr}} + \frac{3p}{4}\frac{l_m}{\sigma l_s l_r}\left[v_s^{\psi_s}\psi_s - (\omega_r - \omega_{\psi_s})\cdot(\psi_s - \psi_r^{\psi_s})\right] \tag{16}$$

$$\frac{dT_e^-}{dt} = -\frac{T_e}{\sigma\tau_{sr}} - \frac{3p}{4}\frac{l_m}{\sigma l_s l_r}\left[(\omega_r - \omega_{\psi_s})\cdot(\psi_s - \psi_r^{\psi_s})\right] \tag{17}$$

The instantaneous stator flux angular frequency, $\omega_{\psi s}$, can be approximated by taking the ratio of the change in angle, θ, and the change in time during the active voltage vector is applied. Since the number of active voltage vectors selected over one synchronous cycle is given by $2\pi f_{tri}/\omega_e$ and the duration of the applied active voltage vectors during each carrier cycle is linearly related to the average duty ratio, $d(t)$, hence:

$$\omega_{\psi_s} = \frac{\Delta\theta}{\Delta t} = \frac{\frac{2\pi\omega_e}{2\pi f_{tri}}}{\frac{d}{f_{tri}}} = \frac{\omega_e}{d} \tag{18}$$

Substituting (18) into (16) and (17), the torque equations can be written as:

$$\frac{dT_e^+}{dt} = -A_t T_e + B_t v_s^{\psi_s} + K_t\left(\frac{\omega_e}{d} - \omega_r\right) \tag{19}$$

$$\frac{dT_e^-}{dt} = -A_t T_e - K_t \omega_r \tag{20}$$

where $A_t = \frac{1}{\sigma\tau_{sr}}$, $B_t = \frac{3p}{4}\frac{l_m}{\sigma l_s l_r}\psi_s$ and $K_t = \frac{3p}{4}\frac{l_m}{\sigma l_s l_r}\psi_s\psi_r^{\psi_s}$ are assumed constant.

Equations (19) and (20) are averaged and simplified to give:

$$\frac{dT_e}{dt} = -A_t T_e + B_t v_s^{\psi_s} d + K_t(\omega_{slip}) \tag{21}$$

Taking the Laplace transform of (21) and re arranging gives (22)

$$\tilde{T}_e = \frac{B_t v_s^{\psi_s}\tilde{d}(s) + K_t\tilde{\omega}_{slip}(s)}{s + A_t} \tag{22}$$

If the slip frequency is neglected, as it is relatively small, the linearized torque loop based on (22) is as shown in Fig. 5.

The PI controller must be designed so that the slope of T_c does not exceed the triangular carrier slope. The slope of T_c is mainly determined by the proportional gain, K_{tp}, of the PI controller, hence the following equations must be satisfied:

$$\text{Absolute slope of the carrier} \geq \left\{-A_t T_e + B_t v_s^{\psi_s} + K_t\left(\frac{\omega_r}{d} - \omega_r\right)\right\} K_{tp}^{+} \quad (23)$$

$$\text{Absolute slope of the carrier} \geq \left|-A_t T_e - K_t \omega_r\right| K_{tp}^{-} \quad (24)$$

In order to ensure proper operation, the smaller value between K_{tp}^{+} and K_{tp}^{-} will be chosen. The integrator gain, K_{ti} is chosen such that the pole of the open loop gain is cancelled.

B. Flux Controller

Equations (10) and (11) show that the flux slopes varies with flux position, are functions of sinus of the angle and repeats for every sector. To simplify the analysis, it will be assumed that the slope is constant during which the flux error status is 1 or 0. Consequently, (25) and (26) are obtained representing the average value of the flux slopes over a sector.

$$\frac{d\psi^{+}}{dt} = \frac{1}{N_f}\sum_{n=0}^{N_f}\frac{2}{3}V_{dc}\sin\left(\frac{\frac{\pi}{3}}{N_f}\right)n = A_\psi \quad (25)$$

$$\frac{d\psi^{-}}{dt} = -\frac{1}{N_f}\sum_{n=0}^{N_f}\frac{2}{3}V_{dc}\sin\left[\left(\frac{\frac{\pi}{3}}{N_f}\right)n + \frac{2}{3}\pi\right] = B_\psi \quad (26)$$

N_f is the number of positive and negative slopes within a sector which equal to $(2\pi f_{trri})/6\omega_e$. Equation (27) gives an average slope of flux:

$$\frac{d\psi}{dt} = (A_\psi - B_\psi)d + B_\psi \quad (27)$$

Introducing small perturbation in ψ and d, the transfer function becomes:

$$\frac{\tilde{\psi}}{d} = \frac{A_\psi - B_\psi}{s} \quad (28)$$

The complete flux loop is shown in Fig. 6.

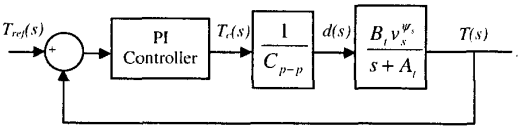

Fig. 5. Linearized torque loop

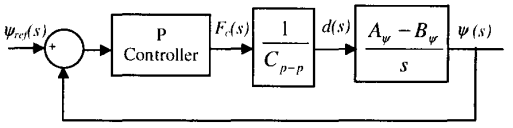

Fig. 6. Linearized flux loop

Equation (28) indicates that the flux loop just requires a proportional controller since the open-loop gain consists of only an integral and a gain. There are two limitations taking into account. Firstly, the slope of the output of the proportional controller must not exceed the triangular slope as shown in (29).

$$\text{Absolute slope of the carrier} \geq K_\psi \frac{d\psi}{dt} \quad (29)$$

According to (10) and (11), the maximum positive slope occurs at $\pi/3$, while the steepest negative slope occurs once the stator flux enter a new sector, i.e.θ = 0°. Secondly, we also have to ensure that the bandwidth is large enough to remove the ripple at 6 × the synchronous frequency (f_e).

V Simulation Results

The proposed controllers and the hysteresis-based controller are simulated using the same induction machine parameters as tabulated in Table I.

For the proposed controllers, the numerical values of the parameters for the torque and flux loops are calculated and listed in Table II. The triangular frequency of the torque and flux controllers are set to 20kHz and 10kHz respectively, each with a peak-peak of 100 units. The values of the controllers' parameters are obtained based on the procedure described previously. The bandwidths of the torque and flux loops are also limited by the triangular waveforms frequency.

TABLE I
PARAMETERS OF INDUCTION MACHINE USED FOR SIMULATION

Stator resistance	10.9 Ω
Rotor resistance	9.5 Ω
Stator self inductance	0.859 mH
Rotor self inductance	0.859 mH
Mutual inductance	0.828 mH
Rated speed	2880 rpm
Pole pair	2
DC link voltage	392 V
Rated flux	0.495 Wb

TABLE II
PARAMETERS FOR THE PROPOSED TORQUE AND FLUX CONTROLLERS

Torque		Flux	
A_t	335	A_ψ	226
B_t	12	B_ψ	226
K_t	6	K_ψ	6900
K_{tp}	862		
K_{ti}	288960		

The widths of the flux and torque hysteresis comparators are set to 5% of their respective rated values.

Fig 7 shows the torque and speed responses of the proposed and hysteresis-based controllers to a square wave torque reference of ±0.5Nm. The figure clearly indicates the reduction in torque ripple in the proposed controller compared to the hysteresis based controller. The results also indicate that the dynamic torque response of the proposed controller is as good as the hysteresis-based controller. Fig. 8(a) and (b) show the zoomed torque responses of the proposed and hysteresis based controllers. The triangular waveform, which is compared with the output signal of the PI controller, is depicted in Fig 8(c). Fig 8(d) shows the output of the hysteresis controller indicating that the non-zero voltage vector is selected during torque reduction. Fig. 9 shows the steady state flux locus for both controllers, clearly indicating the improved locus for the proposed controller. Fig. 10(a) and (b) show the flux responses of the proposed and hysteresis-based controllers, indicating the significant reduction in the ripple. Fig. 10(c) shows the triangular waveform and the output of the P controller for the flux loop while Fig 10(d) show the output of the hysteresis based comparator.

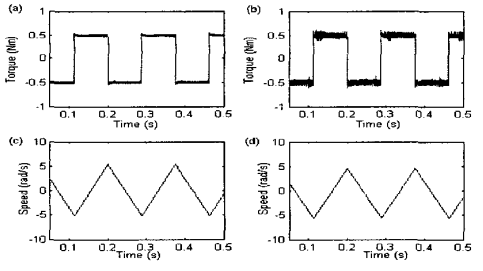

Fig. 7 (a) Torque response for proposed controller, (b) Torque response for hysteresis-based controller, (c) Speed response for proposed controller, (d) Speed response for hysteresis-based controller

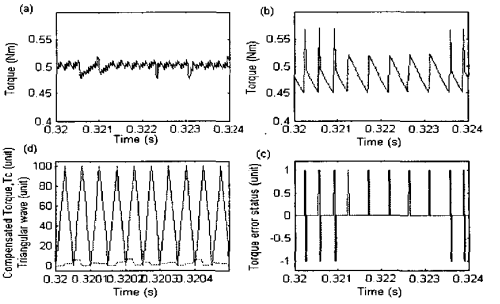

Fig. 8 (a) Zoom in torque response for proposed controller, (b) Zoom in torque response for hysteresis-based controller, (c) Upper triangular waveform and T_c for proposed controller, (d) Torque error status for hysteresis-based controller

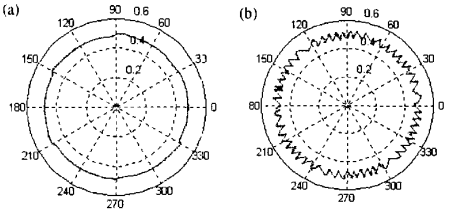

Fig. 9 Steady state flux locus, (a) proposed controller, (b) hysteresis-based controller

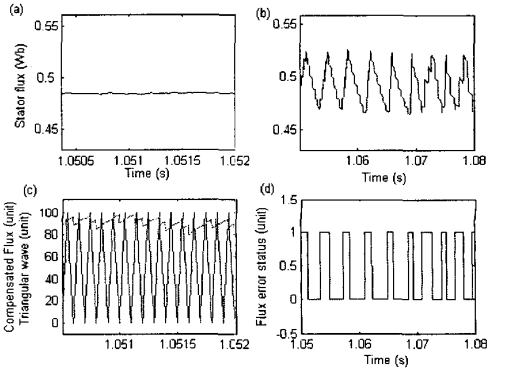

Fig. 10 (a) Stator flux for proposed controller, (b) Stator flux for hysteresis-based controller, (c) Triangular waveform and F_c for proposed controller, (d) Flux error status for hysteresis-based controller

VI. CONCLUSIONS

A new torque and flux controllers with high and constant switching frequency has been proposed. The methodology of the controllers' design has been presented and the simulation results showed that the controllers have managed to reduce the torque and flux ripples significantly. The switching frequency is fixed to the triangular waveform frequency, regardless of the operating conditions. Due to the nature of the controllers,

which are based on waveform comparisons, it is therefore possible to implement them without the need of a fast digital signal processor.

REFERENCES

[1] P. Tiitinen and M. Surandra, "The next generation motor control method, DTC direct torque control", Proceedings of the 1996 International Conference on Power Electronics, Drives and Energy System for Industrial Growth, N. Delhi, India, Vol.1, pp. 37-43, 1996.

[2] I. Takahashi, T. Noguchi, "A new quick-response and high-efficiency control strategy of an induction motor", IEEE Trans. Ind. Appl., Vol. IA-22, No 5, pp. 820-827, 1986

[3] Purcell, A. and Acarnly, P. (1998). "Multilevel hysteresis comparator forms for direct torque control schemes", Electronics Letters, Vol. 34, No. 6, pp. 601-603.

[4] J-W. Kang, D-W Chung and S. K. Sul, "Analysis and prediction of inverter switching frequency in direct torque control of induction machine based on hysteresis bands and machine parameters", IEEE Transactions on Industrial Electronics, Vol. 48, No.3, pp. 545-533, Jun 2001.

[5] D. Casadei, G. Grandi, G. Serra, A. Tani, "Switching strategies in direct torque control of induction machines," in Proc. Of ICEM'94, Paris (F), 5-8 September 1994, pp. 204-209.

[6] J-W. Kang, D-W Chung and S.K. Sul, "Direct torque control of induction machine with variable amplitude control of flux and torque hysteresis bands", International Conference on Electric Machines and Drives IEMD'99, pp. 640-642, 1999.

[7] T. G. Habetler, F. Profumo, M. Pastorelli and L. M. Tolbert, "Direct torque control of induction machines using space vector modulation", Conference Record of the Industry Applications Society Annual Meeting, Vol. 1, pp. 428-436, 1991.

[8] Lixin Tan and M.F. Rahman, "A new direct torque control strategy for flux and torque ripple reduction for induction motors drive by using space vector modulation", 32nd Annual Power Electronics Specialists Conference PESC. 2001, Vol.3, pp. 1440-1445, 2001.

[9] D. Casadei, G. Serra and A. Tani, "Improvement of direct torque control performance by using a discreate SVM technique", 29th Annual IEEE Power Electronics Specialists Conference PESC 98, Vol. 2, pp. 997-1003, 1998.

[10] S. Mir, and M. E. Elbuluk, " Precision torque control in inverter-fed induction machines using fuzzy logic", IEEE-IAS Annual Meeting, pp. 396-401, 1995.

[11] I. G. Bird, and H. Zelaya De La Parra, "Fuzzy logic torque rippli reduction for DTC based AC drives", Electronic Letters, Vol. 33, No.17, pp/ 1501-1502, 1997.

[12] Y. Li, J. Shao and B. Si, "Direct torque control of induction motors for low speed drives considering discrete effect of control and dead-time timing of inveters", IEEE-IAS Annual Meeting, pp. 781-788, 1997.

[13] Purcell, A. and Acarnly, P, "Device switching scheme for direct torque control", Electronics Letters, Vol. 34, No. 4, pp. 412-414, 1998.

[14] T. Noguchi, M. Yamamoto, S. Kondo and I. Takahashi, "High frequency switching operation of PWM inverter for direct torque control of induction motor", Conference Record of the Industry Applications Annual Meeting IAS'97, Vol. 1, pp. 775-780, 1997.

[15] N. R. N. Idris, A. H. M. Yatim, "Reduced Torque Ripple And Constant Torque Switching Frequency Strategy For Direct Torque Control Of Induction Machine", 15th IEEE-Applied Power Electronics Conference and Exhibiton 2000 (APEC 2000), New Orleans, USA, Feb 2000.

[16] J.K. Kang and S.K.Sul, "Torque ripple minimization strategy for direct torque control of induction motor", in Conf. Rec. IEEE-IAS, pp. 438-443, 1998.

[17] J-K. Kang, S-K. Sul, (2001, June). Analysis and prediction of inverter switching frequency in direct torque control of induction machine based on hysteresis bands and machine parameters. IEEE Trans. Ind. Appl., Vol. 48, No. 3, pp. 545-553.

[18] N.R.N.Idris, A.H.M Yatim, N.D. Muhamad and T.C. Ling "Constant frequency torque and flux controllers for direct torque control of induction machines", Accepted for the 34th IEEE Power Electronics Specialist Conference PESC03, Acapulco, Mexico, June 2003.